Exploration of Physicochemical Properties for Commercial and Novel CO Oxidation Catalysts that are used in Life Support Applications

Sudheera Yaparatne[1], Madison McCarthy[2] , and Onur G. Apul [3]
Department of Civil and Environmental Engineering, University of Maine, Orono, ME 04469, USA

John C Graf[4], Lawrence W Barrett[5], Oageng N George[6], and Riley M Reichert[7],
NASA Johnson Space Center & Jacobs JETS Contract, Houston, TX, 77058, USA

Timothy Nalette[8]
NASA Langley Research Center, Hampton, VA 23666

Wenhu Wang [9]
Frontier Institute for Research in Sensor Technologies (FIRST), University of Maine, Orono, ME 04469

and

Seung Soo Lee[10],
Department of Chemical and Environmental Engineering, Yale University, New Haven, CT 06511

The NASA JSC Engineering Technology and Science contract focuses on developing life support and emergency response equipment for space missions. This includes the Contingency Breathing Apparatus (CBA) and Orion Smoke Eater Filter (OSEF), designed to address fire-related particulates and noxious gases aboard the Orion Multi-Purpose Crew Vehicle. However, the existing TDA catalyst (from TDA Research Inc.) in NASA's CBA and OSEF systems is costly and susceptible to damage. Recent advancements have introduced more cost-effective and durable catalysts by various manufacturers. This study extends our previous work by comparing the TDA catalyst with a commercially available CO oxidation catalyst developed by Astrea Materials. The catalyst performance was assessed for CO oxidation across varying temperatures, flowrates, and relative humidity levels. Furthermore, the mechanical strength of both catalysts during handling and mechanistic factors contributing to performance degradation were evaluated. Attrition tests revealed that the TDA catalyst was more prone to dust generation than the Astrea catalyst, which exhibited better resilience in

[1] Postdoctoral research associate, Department of Civil and Environmental Engineering, University of Maine, Orono, ME 04469, USA.
[2]Undergraduate Research Fellow, Department of Civil and Environmental Engineering, and University of Maine, Orono, ME 04469, USA.
[3] Assistant Professor, Department of Civil and Environmental Engineering, and University of Maine, Orono, ME 04469, USA.
[4] Engineer, NASA Johnson Space Center, Houston, TX, 77058.
[5] ECLSS Analysis Technical Lead, Jacob Technology, JSC Engineering, Technology, and Science (JETS).
[6] JETS Project Manager, Jacob Technology, JSC Engineering, Technology, and Science (JETS).
[7] Engineer, NASA Johnson Space Center, Houston, TX, 77058.
[8] Former Chief of Advanced Systems and Technology at United Technologies Aerospace Systems.
[9] Postdoctoral Research Associate, Frontier Institute for Research in Sensor Technologies (FIRST), University of Maine, Orono, ME
04469.
[10] Research Scientist, Department of Chemical and Environmental Engineering, Yale University, New Haven, CT 06511.

attrition and compression tests. The BET surface area of the Astrea catalyst was ~1.5 times that of the TDA counterpart. The performance of the TDA catalyst, in terms of CO oxidation per unit volume of the bed, was superior to that of the Astrea catalyst at different temperatures and humidity levels. ICP and XPS techniques were employed to determine the bulk and surface composition, respectively, of the catalysts. The XPS analysis revealed changes in the catalytic (Au) and support materials when exposed to CO. SEM analysis showed a more agglomerated surface morphology in the Astrea catalyst compared to its TDA counterpart. This study established the significance of systematic XPS, in situ FTIR, and TEM analyses in revealing chemical and morphological changes on the surface and bulk of the catalysts, thereby enabling the identification of the mechanistic causes of their deactivation.

Nomenclature

GHSV	=	Gas hourly space velocities
RH	=	Relative humidity
T	=	Temperature near the catalyst
F_H	=	Feret diameter of the catalyst particles along the horizontal axis
F_V	=	Feret diameter of the catalyst particles along the vertical axis

I. Introduction

Spacecraft fires present a significant concern in planning for both current and future missions. One aspect of fire safety involves post-fire cleanup strategies that include the rapid and effective removal of toxic particulates and gases. Carbon monoxide (CO) is a major toxic gas indicator of a fire emitted due to incomplete combusion.[1] According to NASA standards, the spacecraft's maximum allowable concentration (SMAC) for CO over a long-term period of 1,000 days is 15 ppm.[2] The 1 h CO SMAC threshold level for CBA is set as 425 ppm during a fire event.[3] In alignment with the JSC Engineering Technology and Science (JETS II) National Aeronautics and Space Administration (NASA) contract, efforts are underway to develop life support and emergency response equipment for NASA space flight missions.[4] These projects focus on evaluating the CO oxidation catalyst used in the contingency breathing apparatus (CBA) and Orion smoke eater filter (OSEF). The CBA and OSEF devices are integral components of the environmental control and life support (ECLS) equipment, specifically designed to mitigate particulate matter and harmful gases released during a fire event onboard the Orion multi-purpose crew vehicle (MPCV).

In the domain of effective CO oxidation, noble metal catalysts exhibit enhanced performance at lower temperatures and superior moisture resistance compared to other catalysts.[5–7] Within this group of catalysts, there has been a growing interest in the application of supported gold (Au) catalysts, particularly since the discovery of low-temperature CO oxidation by Haruta et al.[8] Supported Au catalysts have demonstrated higher CO oxidation ability, especially when Au is dispersed and deposited on reducible semiconductor metal oxides, hydroxides of alkaline earth metals, or amorphous ZrO_2.[9] In addition to the increased interest in low-temperature applications, supported Au catalysts have demonstrated enhanced odor and CO removal capabilities in the presence of moisture.[10]

The catalyst presently employed in NASA applications for CBA and OSEF is a gold (Au) catalyst supported on iron oxide, specifically designed for NASA by TDA Research Inc.[3] The TDA catalyst continues to demonstrate comparable performance when compared to newly available commercial catalysts in the removal of CO. However, the TDA catalyst is associated with a significant expense, and previous evaluations have exposed its susceptibility to fracturing and dust generation during packing, transportation, and handling. Over the past 5-10 years, multiple catalyst manufacturers have introduced innovative variations of commercially accessible catalysts, demonstrating enhanced CO oxidation activity and increased durability.

In a prior study, we evaluated the CO oxidation of Astrea Materials catalyst under different gas hourly space velocities (GHSVs), relative humidity (RH) levels, and catalyst temperatures (T).[11] In this current study, we extend our previous work by conducting a comparative analysis of the TDA and Astrea catalysts for CO oxidation under various conditions, including changes in GHSVs, RH, and T. Additionally, we evaluated the mechanical strength of both catalysts during handling and examined the mechanistic causes of performance degradation. Specifically, this paper includes (A) a quantitative assessment of the dusting tendencies of TDA and Astrea catalysts, (B) a comparison of CO removal of TDA and Astrea catalysts at different T, RH, and GHSV levels, and (C) an

assessment of the mechanistic causes for performance degradation of the catalysts at the end of the CO oxidation tests.

II. Materials and Methods

A. Quantitative assessment of the dusting tendencies of TDA and Astrea catalysts

The attrition test was performed using a Benchmark BeadBug^{TM} mini homogenizer (Model D1030-E). In this test, approximately 0.5 g of sieved (ASTM No. 20) Astrea and TDA catalysts (used as bought/received material) coarse particles (> 850 µm) were measured into 2 mL Benchmark plastic tubes and agitated at three different speeds (2800, 3400, and 4000 rpm) for 30 s in a Benchmark BeadBug^{TM} mini homogenizer. After the agitation period, the tube contents were sieved by ASTM No. 20 sieves, and the mass of the coarse particles was measured to determine the loss due to attrition. Percent loss due to attrition was determined according to Equation 1. The attrition tests were repeated 3 times for each catalyst at the 3 different speeds of the homogenizer.

Before and after exposure to the CO oxidation reaction under each condition, TDA and Astrea catalysts (as bought/received material) were analyzed for their size distribution under the dissecting microscope. The size/diameter of 100 particles of each of these catalysts along the vertical axis (F_V) and horizontal axis (F_H) (F: Feret diameters) were measured. Constant rate of strain (CRS) test was performed for the Astrea catalyst (as bought material) at a strain rate of 2.5 % h^{-1} for 25.00 g (Sample height: 1.45 cm, Cell diameter: 5.08 cm) of Astrea catalyst (> 850 µm; ASTM No. 20). This test was performed by following the ASTM D4186/D4186M-12 method[12] under dry conditions. Geotac, Sigma 1 automated load test system equipped with GeoJac digital load actuators was used for this compression test.

$$\textbf{Loss due to attrition (\%)} = \frac{Initial\ mass - final\ mass}{Initial\ mass} \times 100\% \quad \textbf{(Equation 1)}$$

B. Comparison of CO removal efficiency of Astrea and TDA catalysts at varying temperatures, relative humidity, and gas hourly space velocities

TDA and Astrea catalyst CO removal was evaluated and compared at 0 °C, 12 °C, and 25 °C Ts. T experiments were performed at 5.3×10^4 h^{-1} and 1.1×10^5 h^{-1} GHSVs. The catalysts were used as received material for these CO oxidation tests. T experiments were performed at 5.3×10^4 h^{-1} and 1.1×10^5 h^{-1} GHSVs. The T experiments were conducted under low humidity to isolate the effect of temperature on CO removal by the catalyst. For these experiments, RH was kept below 0.5% throughout the experimental period. The CO removal percentages at 15%, 50%, and 85% RH conditions were also measured for both TDA and Astrea catalysts. The RH experiments were performed at 25 °C and 5.3×10^4 h^{-1}. CO oxidation experiments were performed in a fixed-bed glass reactor designed by Ace Glass. The inner diameter of the reactor tube was 1.5 cm, and the packed catalyst bed depth was 2.5 cm (5.00 g TDA catalyst and 3.20 g of Astrea) of catalyst was used in its purchased condition. The volume of the catalyst bed was 4.42 $\times10^{-3}$ L. A thermocouple temperature probe was inserted in the glass reactor to monitor the temperature at the catalyst. The catalyst was placed between pieces of stainless steel wire mesh and quartz wool. The remaining space was homogeneously packed with glass beads, as shown in Figure 1.

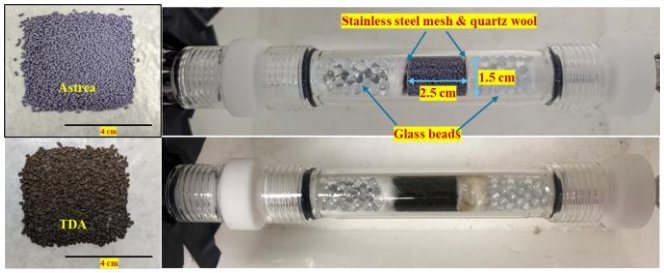

Figure 1. Reactor tube packed with TDA & Astrea catalyst[11]

CO oxidation experiments were started at a CO concentration of around 1000 ppm. The reactor setup for the T and RH experiments is shown in Figure 2. In T experiments, before testing the catalyst activity, a steady CO level (~1000 ppm) was achieved by flowing zero air and CO through the system by opening valves #1 and #4 (valves #3 and#2 closed). The CO removal measurements were started by opening valve #3 and closing valve #4 (#2 is closed for T experiments). RH experiments were conducted by adjusting the water bath temperature to an appropriate level to achieve the desired RH (mixing dry and wet zero air and flowing through the catalyst) by opening valve #2. Similar to T experiments, a steady CO level was achieved by flowing zero air and CO mixture through the system by opening valves #1, #2, and #4 (valve #3 closed). The CO removal measurements were started by opening valve #3 and closing valve #4.

In each of these experiments, CO levels were measured for 60 min. CO removal percentages were calculated from the 5th to the 60th min (at 5-min intervals) to determine the average CO removal under each condition. Three trials were performed for each condition without changing the catalyst, and the average and standard deviation of the three trials were calculated for statistical robustness.

Based on the results obtained for T experiments, as shown in section III B, the amounts of extra Astrea catalyst needed to match the performance of TDA at different temperatures were calculated by considering the volume and mass of the catalyst in the reactor. For this calculation, the results of the experiments performed at $1.1\times10^5\ h^{-1}$ were used.

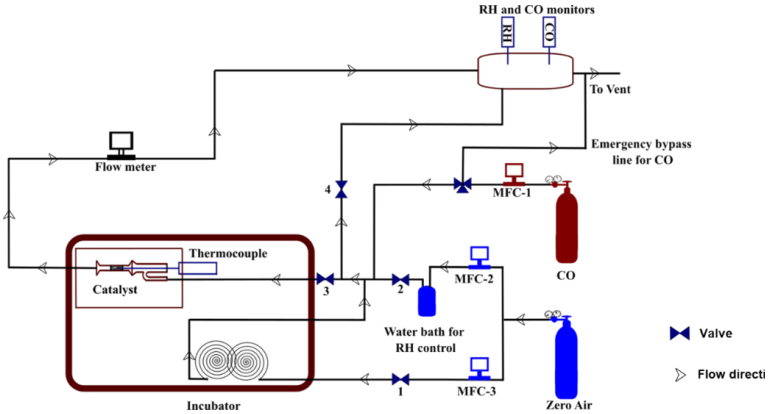

Figure 2. Experimental setup for CO oxidation at different T and RH levels[11]

C. Assessment of mechanistic causes performance degradation at the end of testing

Several material characterization tests were performed to investigate the factors affecting CO oxidation capability and assess the effectiveness of the catalysts. The surface area, pore volume, and pore size distribution of Astrea and TDA catalysts (used for CO oxidation experiments) were measured using Micromeritics ASAP 2020. The Brunauer-Emmett-Teller (BET) and Barrett-Joyner-Halenda (BJH) models were employed to determine the surface area, pore volume, and pore size distribution through nitrogen adsorption/desorption isotherms in Astrea and TDA used catalysts. The catalyst powder samples (about 0.10 g) were first evacuated at 130 °C for 10 h. An adsorption/desorption isotherm curve was collected at 77 K (-196.15 °C) and at relative pressures of N_2 from $P/P_0 < 0.01$ to 0.996, where P_0 is the saturation pressure. BET surface areas were calculated using the adsorption branch of the N_2 sorption isotherms. Moreover, surface area, pore volume, and pore size distribution of the coarse (4000_C) and fine particles (4000_F) after the attrition test at 4000 rpm were also evaluated.

Surface morphology and surface elemental composition were evaluated using a Zeiss NVision 40 scanning electron microscopy (SEM) with energy-dispersive X-ray spectroscopy (EDX). SEM/EDX sample preparation was performed as follows: A small amount of catalyst was scattered over a carbon tape on an aluminum SEM stub. Bulk Au, Fe, and Ti contents of TDA and Astrea catalysts were measured by dissolving the solids in HF and analyzing them with inductively coupled plasma atomic emission spectroscopy (ICP-OES). Surface composition of the catalysts before and after CO oxidation was evaluated using X-ray photoelectron spectroscopy (XPS). XPS was performed on a dual anode VG Microtech X-ray source and a SPECS HSA2000 analyzer. The catalyst samples were spread over carbon tape, placed inside the XPS chamber, and left to evacuate overnight before recording an XPS spectrum. The spectra were processed using Casa XPS software. Astrea and TDA catalysts before and after CO oxidation were characterized through FEI Tecnai Osiris 200 kV transmission electron microscope (TEM). TEM samples (10 mg of the sample in 10 mL of ethanol) were sonicated for a couple of minutes, and 10 µL of the dispersed sample was placed on the TEM grid and dried at room temperature in the air overnight. Surface adsorbed species before and after usage of TDA and Astrea catalysts were analyzed using diffuse reflectance infrared Fourier transform spectroscopy (DRIFT-FTIR) before and after CO oxidation using Nicolet™ iS20 FTIR Spectrometer. A mercury cadmium telluride (MCT) detector was used for IR signal detection.

III. Results and discussions

A. Quantitative assessment of the dusting tendencies of TDA and Astrea catalysts

1. Attrition test with Benchmark BeadBug™ mini homogenizer

The average % losses due to attrition for TDA and Astera at varying vibration speeds are summarized in Table 1 and Figure 3. Error bars indicated in Figure 3 show the standard deviation of the three trials. In this series of test results, the TDA catalyst exhibits higher attrition-related losses than Astrea at each vibration speed, further confirming the fragility of the TDA.

Table 1. Loss due to attrition (%) at different vibration speeds

	% Loss due to attrition		
	Homogenizer speed (rpm)		
Catalyst	2800	3400	4000
Astrea	0.57	0.98	4.93
TDA	4.99	7.18	14.13

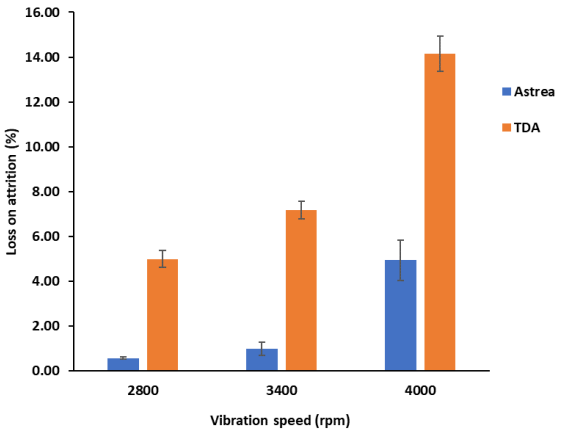

Figure 3. Loss due to attrition TDA vs. Astrea catalyst

2. Size distribution of TDA and Astrea catalysts

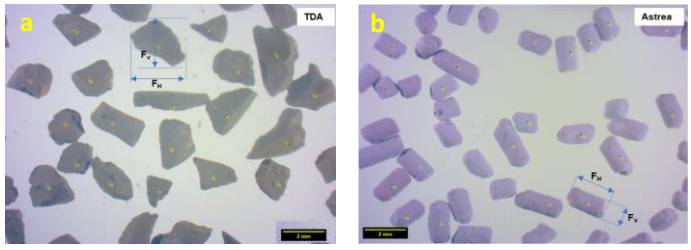

Figure 4. Dissecting microscopy images of (a)TDA and (b) Astrea catalysts

The sizes/diameters of 100 particles of each of these catalysts along the vertical axis (F_V) and horizontal axis (F_H) (Feret diameters) were measured as shown in Figure 4. Size distributions and average catalyst diameters for unused and used TDA and Astrea are shown in Figure 5 and Figure 6, respectively. The average F_H and F_V of TDA before CO oxidation were 1.86 ± 0.51 mm and 1.81 ± 0.49mm, while after usage, the F_H and F_V values came out to be 1.91 ± 0.47 mm and 2.02 ± 0.49 mm respectively (Figure 5). According to one-way ANOVA analysis, there was no significant difference between the TDA F_H values before and after using the catalyst ($p > 0.05$). However, F_V values of TDA showed a significant difference before and after usage according to the one-way ANOVA test ($p < 0.05$). The average F_H and F_V of the Astrea catalyst before CO oxidation were 1.78 ± 0.36 mm and 1.02 ± 0.04 mm, respectively. After the CO oxidation, the respective F_H and F_V values of the Astrea catalyst were 1.85 ± 0.39 mm and 1.01 ± 0.03 mm (Figure 6). According to the one-way ANOVA analysis, there was no significant difference between the before and after F_H values as well as F_V values for the Astrea catalyst.

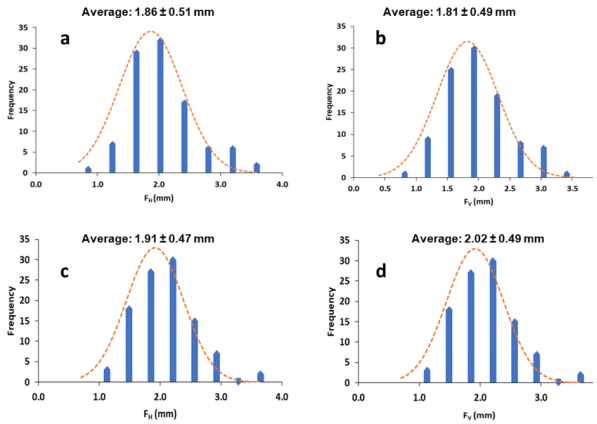

Figure 5. Average Feret diameters (F) and size distributions of TDA catalyst; (a) F_H of unused TDA, (b) F_V of unused TDA, (c) F_H of used TDA, (d) F_V of used TDA

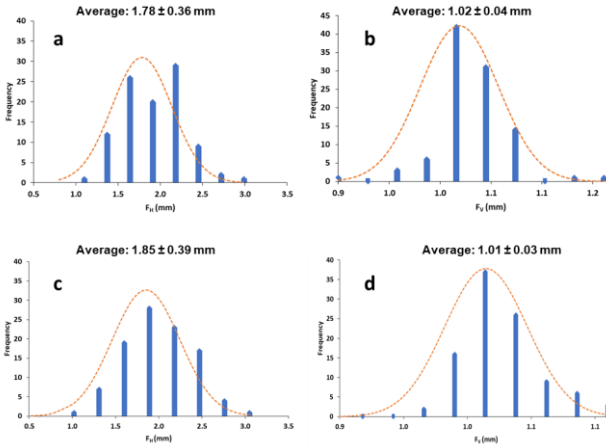

Figure 6. Average Feret diameters (F) and size distributions of Astrea catalyst; (a) F_H of unused Astrea, (b) F_V of unused Astrea, (c) F_H of used Astrea, (d) F_V of used Astrea

3. Constant rate of strain (CRS) test for Astrea catalyst

According to the CRS analysis, Astrea catalysts were able to bear around 490 psi stress at a final strain of 34% without crushing the particles. However, towards the end of the test, it was noted that the catalyst particles had agglomerated under pressure, forming a cohesive, clump-like structure within the stainless-steel cell. The stress-strain curve of this experiment is shown in Figure 7. Further mechanical strength tests, such as compression and CRS tests for TDA, are recommended for evaluating the robustness of the TDA catalyst.

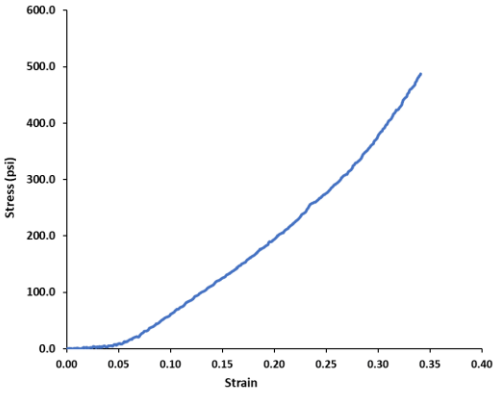

Figure 7. Stress-strain curve of Astrea material (CRS test)

Additionally, robustness and dusting tendency tests for the Astrea catalyst are recommended using CBA and OSEF equipment to assess its viability in real-world applications. While these attrition and compression tests may not precisely simulate the conditions of a launch, in this study, extreme conditions were applied to assess the structural stability of the catalysts both quantitatively and qualitatively. It should be noted that a comparative evaluation of CO oxidation and robustness in TDA and Astrea catalysts under CBA or OSEF configurations for real-space flight launching conditions, normal usage, and during fire events would be beneficial to gain a practical understanding of the structural stability of these catalysts.

B. Comparison of CO removal efficiency of Astrea and TDA catalysts at varying temperatures, relative humidity, and gas hourly space velocities

The average values of CO removal per L of the catalyst bed for T experiments at 5.3×10^4 h^{-1} and 1.1×10^5 h^{-1} GHSVs are shown in Figure 8 and Figure 9, respectively. CO removal percentages from the 5^{th} to the 60^{th} min (every 5 min) were considered to calculate the average CO removal at each condition. Error bars indicate the standard deviation of the three trials. The results of T experiments showed that CO removal per unit bed length of the catalyst is higher in TDA than in the Astrea catalyst. As shown in Figure 8, at 0 °C and 5.3×10^4 h^{-1} GHSV, there is a higher difference in the CO removal between TDA and Astrea catalyst (~30% higher activity in TDA). In contrast, when the temperature increases at the same GHSV, the activity difference between TDA and Astrea decreases (~6 higher activity for TDA compared to Astrea catalyst at 12 °C and 25 °C). The same trend was observed for the higher GHSV

1.1×10^5 h^{-1} T experiments. TDA shows around 37%, 10%, and 13% higher activity compared to Astrea at 0 °C, 12 °C and 25 °C respective temperatures at GHSV 1.1×10^5 h^{-1}. The average values of CO removal per L of the catalyst bed for RH experiments at 1.1×10^5 h^{-1} GHSVs are shown in Figure 10. Error bars indicate the standard deviation of the three trials. The results of the RH experiments show that compared to the Astrea catalyst, the TDA catalyst can function better at higher RH levels. When RH was increased from 15% to 85%, CO removal of Astrea decreased from 3.65×10^{-2} mol min^{-1} L^{-1} to 3.49×10^{-2} mol min^{-1} L^{-1} (~5% decrease), while only a 0.3% decrease was observed for TDA. Moreover, as demonstrated in our previous study[11], the CO oxidation efficiency decreased over time and was further reduced with successive trials in this study. Possible reasons for this deactivation were discussed in section C.

The Astrea catalyst exhibited a lower CO removal percentage of 49.3% at 0 °C and a GHSV of 1.1×10^5 h^{-1} within 1 h compared to all other conditions in this study (Figure 9). At this removal rate, the CO concentration exceeded 500 ppm, which is higher than the recommended SMAC threshold levels for CBA (425 ppm).[3] However, it's important to note that under all other conditions tested for both Astrea and TDA catalysts, a higher CO removal percentage (above ~66%) was achieved, resulting in lower CO levels than the recommended SMAC threshold levels for CBA.

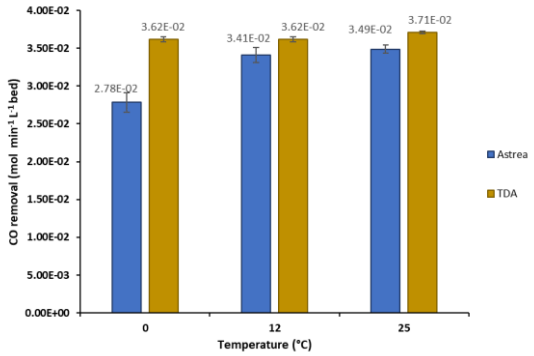

Figure 8. CO removal comparison between TDA and Astrea at different T per L of bed volume at GHSV 5.3×10^4 h^{-1}

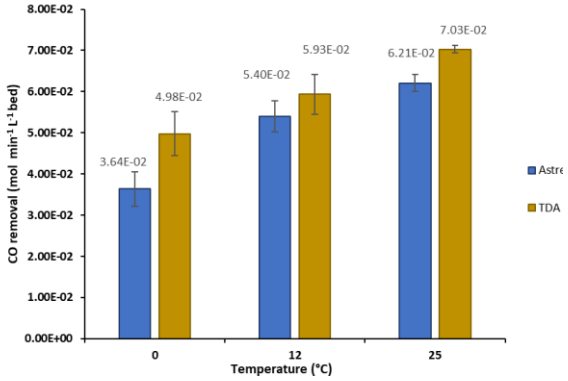

Figure 9. CO removal comparison between TDA and Astrea at different T per L of bed volume at GHSV 1.1×10^5 h^{-1}

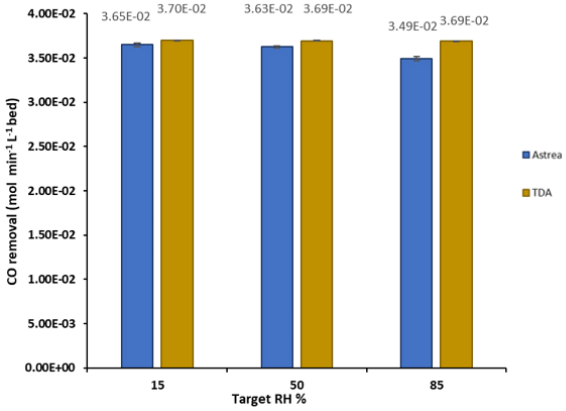

Figure 10. CO removal comparison between TDA and Astrea at different RH per L of bed volume at GHSV 1.1×10^5 h^{-1}

Table 2 shows the volumes of the Astrea catalyst needed to match the performance of the TDA catalyst under the same reactor configuration (Initial volume of the catalyst bed 4.42 $\times 10^{-3}$ L). Moreover, the corresponding increased bed depth of the catalyst values and masses of the Astrea catalyst at these increased volumes are shown in Table 2, considering the bulk density of Astrea.

Table 2. Required volume, increased bed depth of the catalyst, and masses of the Astrea catalyst to match the TDA activity at 1.1×10^5 $h^{-1}$for T experiments

Temperature (°C)	The volume needed to have the same activity (L)	The amount of bed depth should be increased (cm)	Mass (g)
0	6.04×10^{-3}	0.92	4.38
12	4.85×10^{-3}	0.25	3.52
25	5.00×10^{-3}	0.33	3.62

In order to verify the validity of the above estimates, CO oxidation at 0 °C and 1.1×10^5 h^{-1} GHSV was performed using 6.04×10^{-3} L volume of Astrea catalyst (4.38 g and 0. 92 cm bend length increase) to match the performance of TDA. The results of this experiment are shown in Figure 11.

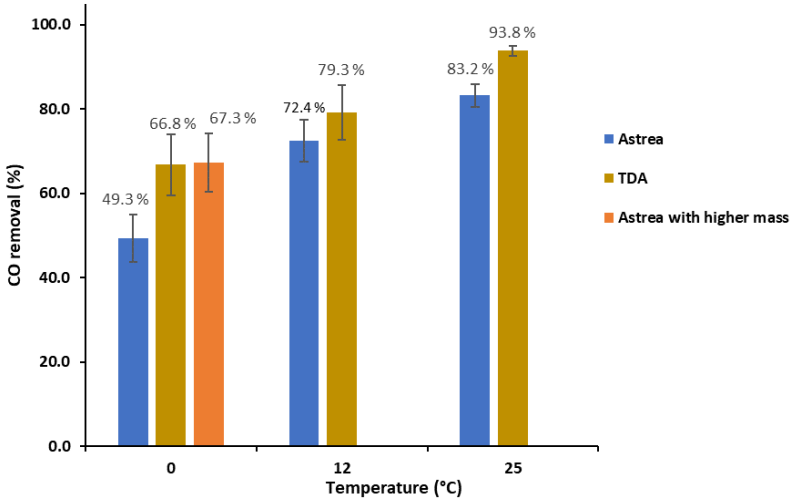

Figure 11. CO removal comparison between TDA and Astrea at different T per L of bed volume at GHSV 1.1×10^5 h^{-1} and the experiment with higher mass of Astrea to match the performance of the TDA at 0°C

C. Mechanistic cause assessment of performance degradation at the end of testing

1. BET surface area, BJH pore volume, and pore diameter

As shown in Figure 12, the surface area of the Astrea catalyst is 1.54, 1.51, and 1.60 times higher than the TDA catalyst for 0, 4000_C, and 4000_F samples, respectively. These results show no considerable decrease in the surface area before and after the attrition test, suggesting no clogging of the catalyst pores due to attrition. The pore volume and average pore diameters of the particles before and after the attrition test further confirm (Figure 13 and Figure 14) that there is no disturbance of the porous structure of both catalysts upon vigorous attrition.

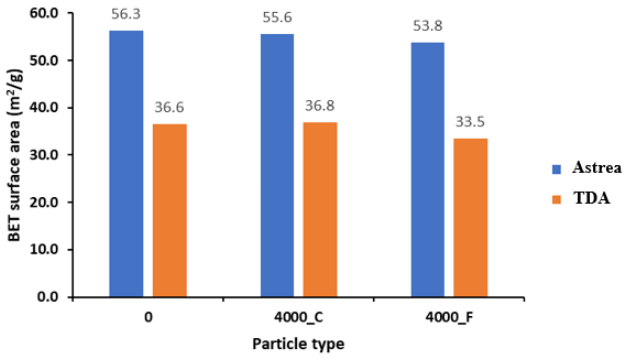

Figure 12. BET surface area of catalysts before (0) and after attrition test (4000_C: coarse particles, 4000_F: fine particles)

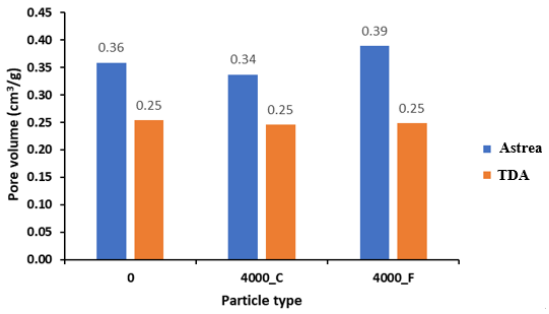

Figure 13. BJH pore volume of catalysts before (0) and after attrition test (4000_C: coarse particles, 4000_F: fine particles)

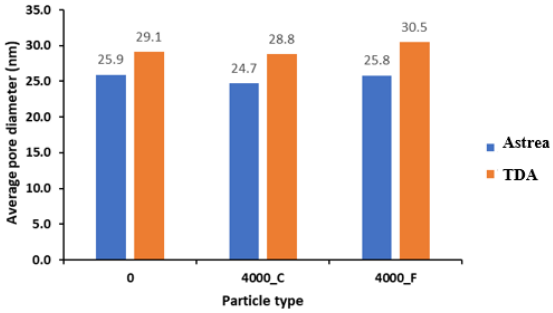

Figure 14. Average pore diameter of catalysts before (0) and after attrition test (4000_C: coarse particles, 4000_F: fine particles)

2. *Scanning electron micrographs (SEM) and Energy-dispersive X-ray spectroscopy (EDX)*
SEM micrographs of the used catalysts show that TDA has a more organized morphology on the surface than the Astrea. SEM of Astrea shows that it has more agglomerations on the surface (Figure 15). EDX results of these samples show a reasonably homogeneous distribution of Fe and Au on TDA and Ti and Au on Astrea surfaces. According to the EDX analysis, the elemental composition (atom ratio) calculated Au/support oxide mass ratio of the surface (~1 µm depth) for TDA was 0.08 (w/w) and 0.06 (w/w) for Astrea. This shows that TDA has slightly higher Au than Astrea on the surface.

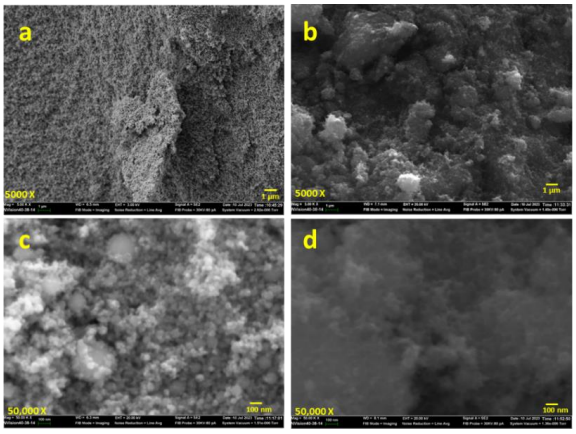

Figure 15. SEM of TDA and Astrea (a)TDA low magnification, (b)TDA high magnification, (c) Astrea low magnification, (d) Astrea high magnification

3. *Bulk composition of TDA and Astrea (ICP-OES)*

Bulk composition showed that Au/Support oxide mass ratios of TDA and Astrea were 0.05 and 0.04 w/w, respectively (Table 3). It is important to identify the effect of the Au/oxide support (w/w) composition on both the bulk and surface of the catalyst since it influences the distribution of Au on the support, which may, in turn, affect the efficiency of CO oxidation activity.[13] While the weight percentage of Au and the Au/oxide support are significant factors for efficient CO oxidation, it is important to note that catalyst activity is also influenced by factors such as the type of support, the structure of the contact area between Au particles and the support, the size of Au particles, and the presence of moisture.[14] Furthermore, catalyst optimization can be achieved by studying the composition, as the supported metal oxide influences epitaxy, particle adhesion, and electronic band bending. These factors, in turn, alter both the dynamic and static behavior of the nanoparticles, in this case, Au nanoparticles.[15] Further structural characterization, focusing on the factors mentioned above, is necessary to explore the optimized compositions of the TDA and Astrea catalysts and compare their abilities for CO removal.

Table 3. The bulk composition of Au and support oxide metal determined from ICP-OES

Catalyst	Au% (w/w)	Fe% (w/w)	Ti % (w/w)	Bulk (ICP) Au/Support (w/w)
TDA	3.39	66.6	n/a	0.05
Astrea	2.11	n/a	53.8	0.04

4. Surface composition by X-ray photoelectron spectroscopy (XPS)

Atomic compositions and mass ratios of the catalysts on the surface are shown in Table 4. The XPS surface elemental composition shows that the Au/Support mass ratio of TDA_{New} and TDA_{Used} catalysts were 0.37 and 0.33, respectively. The Au/Support mass ratio of $Astrea_{New}$ and $Astrea_{Used}$ catalysts were 0.10 and 0.17, respectively. Compared to bulk composition, more Au is detected on the surface of both catalysts. Further analysis is needed to determine any migration of Au onto the surface upon the usage of the catalysts and its effect on CO oxidation. The "New" catalysts mentioned here were before exposed to CO oxidation, and the "Used" catalysts that were analyzed here were exposed to CO (1000 ppm) for 6 h at room temperature and GHSV 1.1×10^5 h^{-1}.

Table 4. The surface composition of new and used catalysts determined from XPS

	Atom%			Surface atom ratio	Surface weight ratio (w/w)
Catalyst	**Au%**	**Fe%**	**Ti %**	**Au/Support**	**Au/Support**
TDA_{New}	0.82	7.77	n/a	0.10	0.37
TDA_{Used}	0.57	6.13	n/a	0.09	0.33
$Astrea_{New}$	0.33	n/a	14.1	0.02	0.10
$Astrea_{Used}$	0.58	n/a	14.0	0.04	0.17

Figure 16(a) and (b) show the Fe 2*P* spectra of the TDA_{New} and TDA_{Used} catalysts. There is a clear difference between the Fe 2*p* spectra of new and used catalysts. This indicates that TDA Fe speciation on the surface changes upon exposure to CO. According to previous research, it has been identified that FeO in FeO/Au catalysts transforms to Fe_2O_3, Fe_3O_4, and carbon-containing iron species (FeCx) due to the exposure of CO.[16] Prior studies on CO oxidation under gold/iron oxide catalysts showed that catalyst activity changes depending on the oxidation state of the iron on the support.[16] Further analysis is required to determine the iron speciation on the substrate during CO oxidation in the TDA catalyst studied. Figure 16 (c) and (d) show the Ti 2*p* peak spectra of the Astrea catalyst. Peaks for Ti^{4+} (Ti 2*p* ½ and 2*p 3/2 doublet)* of $Astrea_{New}$ were observed at 458.8 eV and 464.4 eV, and $Astrea_{Used}$ peaks were observed at 458.4 eV, 464.3 eV. Further analysis is needed to confirm whether the slight difference in peak position values between the new and used Astrea catalysts demonstrates the presence of two separate chemical and electronic states for Ti in the TiO_2 support. It has been identified that the presence of Ti^{3+} species indicates the oxygen vacancies on the TiO_2 catalyst.[17] Oxygen vacancies are important for the catalyst activity since they favor O_2 activation, which in turn facilitates the CO oxidation reaction.[17]. Based on these preliminary results, it's important to assess any changes in Ti^{3+} in Astrea TiO_2 before and after exposure to CO, as this could be a potential cause of catalyst deactivation. Further analysis is required to confirm the chemical and electronic alterations in Au, Fe, and Ti within these catalysts upon exposure to CO. Further analysis of XPS spectra for gold is recommended, as it appears that the abundance of different oxidation states (slightly oxidized gold: $Au^{+\delta}$ or metallic gold: Au^0) in the catalyst plays a significant role in controlling the catalyst's activity and deactivation. Moreover, further studies on the effect and changes of the support oxide are also suggested since prior studies show different CO oxidation extents for the catalysts with the same gold particle size distributions on different supports.[18] One commonly acknowledged mechanism for the influence of the support oxide involves changes in oxygen adsorption and activation during the CO oxidation reaction. These changes are influenced by oxygen vacancies on semiconductor materials and alterations in the conducting properties of these support oxides.[19,20] In addition to its direct involvement in the reaction, the catalyst support can indirectly influence CO oxidation by affecting the shape and size of the Au nanoparticles during catalyst preparation. This influence occurs via metal-support interactions, inducing strain in the Au nanoparticles, facilitating

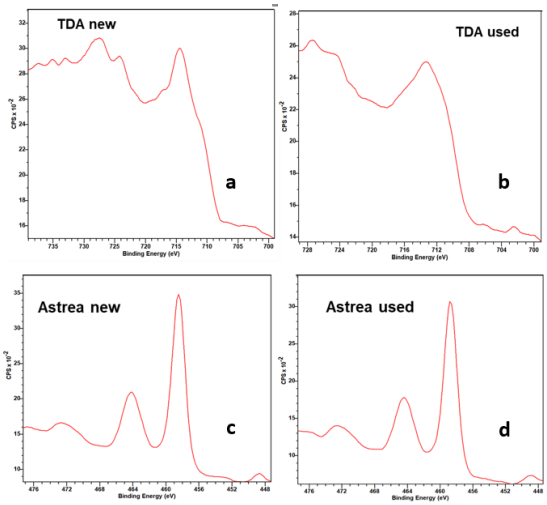

Figure 16. XPS spectra of (a) TDA_{New} Fe 2*p*, (b) TDA_{Used} Fe 2*p*, (c) $Astrea_{New}$ Ti 2*p*, (d) $Astrea_{Used}$ Ti 2*p*

charge transfer to or from the Au nanoparticles, or stabilizing ionic Au species.[21] Therefore, it would be worthwhile to evaluate alterations of the support oxide with the use of the catalyst to predict the catalyst deactivation and regeneration.

5. Transmission electron microscope (TEM) analysis for gold particle size

TEM images of new and used catalysts are shown in Figure 17. Small darker contrast spots within the light contrast larger particles are identified as the gold clusters in both TDA and Astrea.[22] Previous research has reported that the size of gold particles substantially affects catalytic activity, with better activity demonstrated when the gold particle sizes are smaller than 5 nm.[22,23] The size of the gold particle can be used as an essential parameter for efficient catalytic activity. Au particle size distribution of the new and used catalysts could further elucidate the mechanistic causes of catalyst deactivation.

In the analyzed samples, there needed to be more Au particles to conduct a statistically robust analysis of size distribution and observe any differences in size between unused and used catalysts. The average sizes/diameters of the identified gold particles in TDA and Astrea catalysts are shown in Figure 18. In all of the samples, it can be seen that the average size is at below 10 nm in both new and used samples.

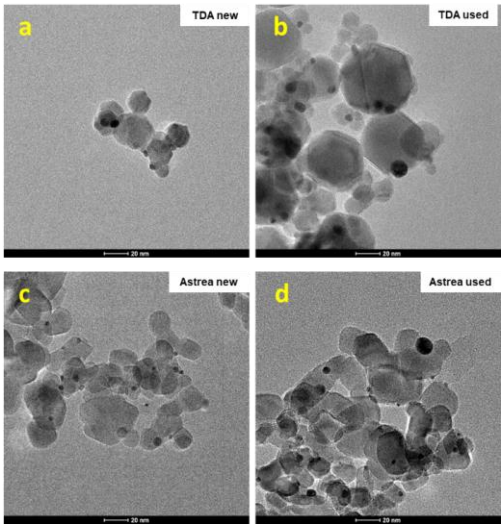

Figure 17. TEM images of (a) TDA_{New}, (b) TDA_{Used}, (c) $Astrea_{New}$, (d) $Astrea_{Used}$

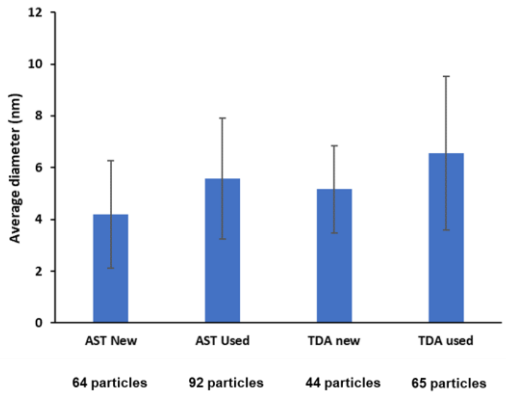

Figure 18. TEM images of (a) TDA_{New}, (b) TDA_{Used}, (c) $Astrea_{New}$, (d) $Astrea_{Used}$

6. Surface adsorbed species of before and after usage; DRIFT -FTIR analysis

According to prior surface analysis studies on CO oxidation catalysts have shown the accumulation of carbonate/carbonate-like species on these catalysts[24,25]. These carbonate species can be bidentate and monodentate[25–27](1800-1200 cm^{-1} wave number region). TDA and Astrea catalysts (New and Used) were analyzed using diffuse reflectance infrared Fourier transform spectroscopy (DRIFT-FTIR) due to the DRIFT surface-sensitive nature and capability to detect subtle alterations on irregular surfaces, selecting it over alternative FTIR techniques. Additionally, the use of a Mercury Cadmium Telluride (MCT) detector was preferred for IR signal detection. MCT detectors offer superior signal-to-noise ratios and considerably faster response times compared to DTGS detectors.

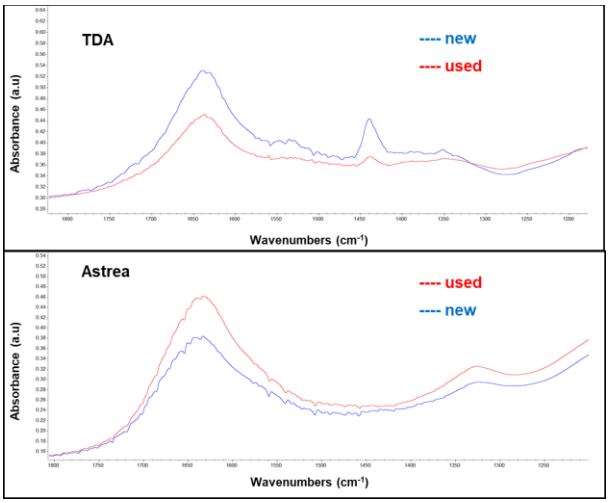

Figure 19. DRIFT_FTIR spectra of TDA and Astrea new and used catalysts

DRIFT spectra of the carbonate regions of TDA and Astrea catalysts are shown in Figure 19**.** According to the current analysis, the Astrea catalyst did not significantly differ between the new and used catalysts. New and used TDA catalysts showed intensity differences in the two prominent peaks in the 1800-1200 cm^{-1} region. However, it is difficult to conclude whether these peaks arise from coordinated carbonate or non-coordinated carbonate species on the catalyst. Non-coordinated carbonate species on the catalyst can also arise without a CO oxidation reaction. Because it is challenging to detect surface-adsorbed species at room temperature and after the reaction has occurred, it is recommended to perform DRIFT measurements simultaneously (*In situ* reaction monitoring) with the ongoing reaction.

IV. Conclusion

In this study, the attrition test revealed that the TDA catalyst tended to dust more than the Astrea material. Astrea catalyst demonstrated better robustness against attrition and compression tests. The TDA catalyst exhibits higher activity in both T and RH experiments than the Astrea catalyst when comparing CO oxidation per unit volume of the catalyst bed. The Astrea catalyst showed a slightly higher (~1.5 times) BET surface area than the TDA catalyst. Usage and vigorous attrition did not significantly change the BET surface areas of both catalysts, and clogging of catalyst pores that can lead to lowering the activity cannot be expected based on these results. SEM analysis showed that Astrea has more agglomerated surface morphology than TDA catalyst. This difference may indicate the robustness/mechanical strength difference between TDA and Astrea.

There is a clear difference between the Fe 2*p* spectra of new and used catalysts. This indicates that TDA Fe speciation on the surface changes upon exposure to CO. The difference in XPS peak position values between the new and used Astrea catalyst confirms the presence of two separate chemical and electronic states for Ti in the TiO_2 support. The preliminary findings of this study show the importance of assessing any changes in Ti^{3+} in Astrea TiO_2 before and after exposure to CO, as this could be a potential cause of catalyst deactivation. Additional investigation is needed to validate the chemical and electronic changes in Au, Fe, and Ti within these catalysts when exposed to CO. In all the samples, it is evident that the average size does not exceed 10 nm in both new and used samples, according to TEM. Further and thorough analysis of the size of Au particles is necessary, as the Au particle size distribution of both the new and used catalysts could provide additional insights into the mechanistic causes of catalyst deactivation. New and used TDA catalysts showed intensity differences in the DRIFT-FTIR analysis. Nevertheless, determining whether these peaks originate from coordinated carbonate or non-coordinated carbonate species on the catalyst poses a challenge. Therefore, using DRIFT-FTIR in situ is recommended to examine surface-adsorbed species closely in real-time, which will help identify the mechanistic causes of catalyst deactivation.

Acknowledgments

The authors gratefully acknowledge the funding NASA and Jacobs Labs provided for the CO oxidation evaluation project. Thanks to Dr. Emma Perry, Electron Microscopy Laboratory Manager at the University of Maine, for TEM and SEM analysis. We also appreciate the support from Dr. Luis Zambrano Cruzatty and Rakesh Pandith of the Civil and Environmental Engineering Department at the University of Maine during the CRS analysis. Dr. Biran Frederick and Andrew Boucher from the Department of Chemistry at the University of Maine for conducting the BET surface area analysis. Furthermore, our thanks are extended to Laurel Grosjean, Research Engineer at the Forest Bioproducts Research Institute, University of Maine, for her assistance with DRIFT analysis.

References

[1] W. K. Cheung, Y. Zeng, S. Lin and X. Huang, *Fire Safety Journal*, 2023, **140**, 103895.
[2] V. E. Ryder, *Spacecraft Maximum Allowable Concentrations for Airborne Contaminants: Revison A*, 2020.
[3] C. H. Cragg, J. C. Graf and A. Hobbs, *Risk Reduction of Orion Multi-Purpose Crew Vehicle (MPCV) Program Government-Furnished Equipment for Environmental Control and Life Support (ECLS)*, NASA Langley Research Center, 2021.
[4] NASA Awards Engineering, Technology, Science Contract - NASA, https://www.nasa.gov/news-release/nasa-awards-engineering-technology-science-contract/, (accessed February 4, 2024).
[5] O. Rosseler, C. Ulhaq-Bouillet, A. Bonnefont, S. Pronkin, E. Savinova, A. Louvet, V. Keller and N. Keller, *Applied Catalysis B: Environmental*, 2015, **166–167**, 381–392.
[6] D. W. Kwon, P. W. Seo, G. J. Kim and S. C. Hong, *Applied Catalysis B: Environmental*, 2015, **163**, 436–443.
[7] N. Imanaka, T. Masui, H. Imadzu and K. Yasuda, *Chem. Commun.*, 2011, **47**, 11032.
[8] M. Haruta, T. Kobayashi, H. Sano and N. Yamada, *Chemistry Letters*, 1987, **16**, 405–408.
[9] M. Haruta, S. Tsubota, T. Kobayashi, H. Kageyama, M. J. Genet and B. Delmon, *Journal of Catalysis*, 1993, **144**, 175–192.
[10] M. Daté and M. Haruta, *Journal of Catalysis*, 2001, **201**, 221–224.
[11] S. Yaparatne, M. McCarthy, L. Nicoloro, N. R. Fisher, O. G. Apul, J. C. Graf, L. W. Barrett and O. N. George, Calgary, Canada, 2023.
[12] M. E. Landon, C. Marchetti and D. J. DeGroot, *Geotech. Test. J.*, 2018, **41**, 425–433.
[13] A. Moreno-Martell, B. Pawelec, R. Nava, N. Mota, L. Escamilla-Perea, R. M. Navarro and J. L. G. Fierro, *Materials (Basel)*, 2018, **11**, 948.
[14] X. Wang, A. Rosspeintner, A. Ziarati, J. Zhao and T. Bürgi, *Nat Commun*, 2022, **13**, 5458.
[15] Z. R. Mansley, R. J. Paull, L. Savereide, S. Tatro, E. P. Greenstein, A. Gosavi, E. Cheng, J. Wen, K. R. Poeppelmeier, J. M. Notestein and L. D. Marks, *ACS Catal.*, 2021, **11**, 11921–11928.
[16] L. Yu, Y. Liu, F. Yang, J. Evans, J. A. Rodriguez and P. Liu, *J. Phys. Chem. C*, 2015, **119**, 16614–16622.
[17] X. Qin, M. Chen, X. Chen, J. Zhang, X. Wang, J. Fang, H. He and C. Zhang, *Applied Catalysis B: Environmental*, 2023, **330**, 122663.
[18] M. Comotti, W.-C. Li, B. Spliethoff and F. Schüth, *J. Am. Chem. Soc.*, 2006, **128**, 917–924.
[19] M. M. Schubert, S. Hackenberg, A. C. van Veen, M. Muhler, V. Plzak and R. J. Behm, *Journal of Catalysis*, 2001, **197**, 113–122.
[20] R. Meyer, C. Lemire, Sh. K. Shaikhutdinov and H.-J. Freund, *Gold Bull*, 2004, **37**, 72–124.
[21] D. Yao, H. Yang, Q. Hu, Y. Chen, H. Chen and P. T. Williams, *Applied Catalysis B: Environmental*, 2021, **280**, 119413.
[22] F. Boccuzzi, A. Chiorino, M. Manzoli, P. Lu, T. Akita, S. Ichikawa and M. Haruta, *Journal of Catalysis*, 2001, **202**, 256–267.
[23] N. Lopez, T. V. W. Janssens, B. S. Clausen, Y. Xu, M. Mavrikakis, T. Bligaard and J. K. Nørskov, *Journal of Catalysis*, 2004, **223**, 232–235.
[24] M. C. Kung, R. J. Davis and H. H. Kung, *J. Phys. Chem. C*, 2007, **111**, 11767–11775.
[25] Y. Denkwitz, Z. Zhao, U. Hörmann, U. Kaiser, V. Plzak and R. J. Behm, *Journal of Catalysis*, 2007, **251**, 363–373.
[26] M. Haruta, *CATTECH*, 2002, **6**, 102–115.
[27] L. Li, A. Wang, B. Qiao, J. Lin, Y. Huang, X. Wang and T. Zhang, *Journal of Catalysis*, 2013, **299**, 90–100.